Design Method to Minimize Current Stress for Auxiliary Resonant Commutated Pole Inverter

Mingi Oh and Iqbal Husain
Department of Electrical and Computer Engineering, North Carolina State University, Raleigh, NC, USA

***Abstract*—The auxiliary resonant commutated pole (ARCP) inverter is an attractive technology for electric vehicle traction inverter applications since it can eliminate most of the switching losses and improve the overall efficiency. However, the selection of resonant circuit elements significantly impacts the inverter's performance. This paper proposes a resonant circuit element selection method that reduces current stress in the auxiliary resonant circuit of an ARCP inverter and helps to achieve a high efficiency. The current stress is reduced by 20.8% and 48.3% compared to previously reported methods and improves the overall efficiency between 0.6% to 9.5% depending on the load. Simulations were conducted using a 45kW, 3-phase, 700V system in LTspice and PLECS to validate the proposed method. The simulation outcomes indicate that the proposed approach is efficient and can be applied to the design and implementation of ARCP inverters. By carefully selecting the components in the auxiliary circuit, the proposed method enables achieving both reduced current stress and improved efficiency.**

***Index Terms*—Auxiliary commutated pole(ARCP), Soft switching, Electric vehicle, Resonant convereter**

I. Introduction

The increasing popularity of electric vehicles (EVs) has led to significant changes in the business strategies of automakers due to government regulations and incentives. For instance, several countries have announced their plans to prohibit the sale of internal combustion engine (ICE) vehicles in the coming years. Table I provides some examples of such regulations.

TABLE I: Government Regulations [1]

Location	regulation
CA, USA	Prohibition of ICE vehicle sales from 2035
Italy	Prohibition of ICE vehicle sales from 2030
Sweden	Only zero-emission vehicles (ZEVs) allowed for new vehicle sales from 2030
Denmark	Only ZEVs allowed for new vehicle sales from 2035
Spain	Only ZEVs allowed for new vehicle sales from 2040
France	Prohibition of new ICE vehicle sales from 2040

The traction inverter is a critical component of an EV that converts the DC power from the battery into AC power that drives the motor, while also controlling the motor's speed and torque. To achieve high power density, low cost, and high efficiency, researchers have focused on developing inverters with emerging power devices and alternative converter topologies and controls. One method is to use wide bandgap (WBG) devices, such as silicon carbide (SiC) MOSFETs and gallium nitride (GaN) high-electron mobility transistors, instead of the traditional silicon (Si) IGBTs. WBG devices have lower switching losses, resulting in improved inverter performance [2]–[4].

Another approach to improving inverter performance is to utilize soft-switching inverters with advanced controls that can significantly reduce switching losses and increase overall efficiency [5]. There are three primary categories of soft-switching inverters: DC-side, AC-side, and triangular current mode (TCM). DC-side soft-switching technology involves the use of an auxiliary circuit between the input source and the three-phase top and bottom rails, while AC-side soft-switching technology involves an auxiliary circuit at each phase. TCM technology, on the other hand, does not require any additional circuit for soft-switching if the inverter has an AC filter. Each of these technologies has its advantages and disadvantages [6]–[10].

The auxiliary resonant commutated pole (ARCP) inverter, which belongs to the AC-side topology, is an attractive proposition for traction inverters since the control and implementation are not too complex compared with the other soft-switching inverter. It has been extensively studied since its development in the 1990s. ARCP inverters can improve efficiency by eliminating most switching losses, allowing for high switching frequencies and reducing cooling requirements. The ARCP topology consists of a resonant circuit in each phase, comprising of two switches, one resonant inductor, and two snubber capacitors. Split DC link capacitors are also required [11]–[14].

Appropriate design of the resonant components, i.e., the resonant inductor and snubber capacitor is critical for achieving the desired resonant time, maximum resonant current, and efficiency. However, few papers have provided a method for selecting these components. The conventional approach is to choose the highest value of snubber capacitor to decrease the turn-off loss. However, since ARCP can eliminate most of the switching losses, this method is not optimal. Another method discussed in [14] only considers EMI attenuation, while the method proposed in [15] does not account for all constraints.

In this paper, we propose a method for selecting resonant circuit elements. We begin by introducing the ARCP topology and operation in Section II. Section III proposes a method for selecting resonant circuit elements. The proposed method considers all constraints and aims to minimize the resonant circuit current. Section IV exhibits simulation results to confirm the proposed method's effectiveness, and Section V provides concluding remarks.

©2023 KIPE

II. ARCP TOPOLOGY AND OPERATION

A. ARCP Topology

The 3-phase ARCP inverter is one of the AC-side topologies which combines three single-phase ARCP topologies to form a 3-phase system shown in Fig. 1. It was first introduced by R.W. De Doncker in 1990 [12]. Each single phase in the 3-phase ARCP inverter is made of a resonant circuit with two auxiliary switches, S_{x1} and S_{x2}, a resonant inductor, L_r, and two snubber capacitors, C_{r1} and C_{r2}. The resonant circuit operates to achieve zero voltage switching (ZVS) and zero current switching (ZCS) of the switches. To ensure proper operation of the 3-phase ARCP inverter, the DC link voltage should be divided into two capacitors.

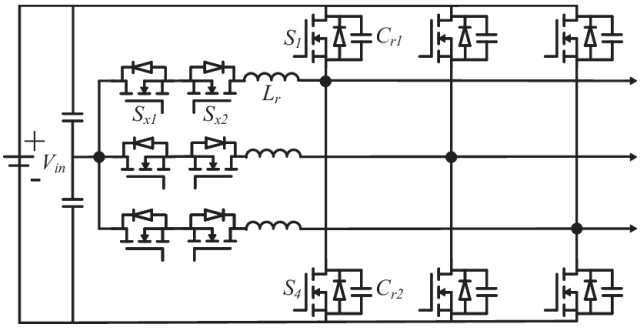

Fig. 1. Three-phase ARCP topology.

B. ARCP Operation

The operation of the ARCP can be divided into six cases depending on the switch operating conditions, and the direction and magnitude of the load current as shown in Fig. 2. The first classification is based on a comparison of the reference voltage of the phase voltage from the controller and the triangle voltage for PWM operation. The second classification depends on the phase current direction. The last classification is determined by whether the load current exceeds the threshold current. The threshold current is the amount of current that can discharge all the energy of the snubber capacitor during the dead-time of the switch without using a resonant circuit. This paper focuses only on Case 1 in Fig. 2, which involves turning on the top switch and positive load current.

Fig. 3 depicts the ideal waveform of the ARCP circuit, which includes the gating signals of the main and auxiliary switches, the resonant current, the current of the main switches, and the voltage of the snubber capacitor, which is ideally equivalent to the voltage of the main switches. The commutation process of the ARCP is illustrated in Fig. 4 [13]. At the beginning of the commutation process (corresponding to t_0 to t_1 in Fig. 3), the resonant circuit is inactive, and the bottom switch (S4) is turned on while the top switch (S1) is turned off. Next, as shown in Fig. 4b (corresponding to t_1 to t_2 in Fig. 3), the auxiliary switch is turned on, and the resonant current increases to match the load current. The resonant current is then further boosted by the boost current to compensate for the resonant circuit loss, as seen in Fig. 4c

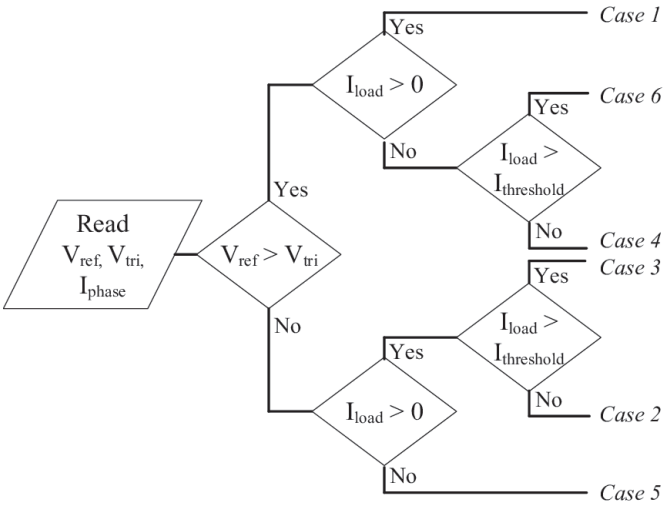

Fig. 2. ARCP operation case.

(corresponding to t_2 to t_3 in Fig. 3). Subsequently, as depicted in Fig. 4d (corresponding to t_3 to t_4 in Fig. 3), the bottom switch is turned off, and the resonant circuit operates alone. During this time, the voltage of the snubber capacitor attached to the top switch drops to 0V, while the voltage of the bottom switch increases by V_{DC}. When the voltage of the top switch reaches 0V, the top switch (S1) is turned on, which triggers the ZVS turn-on operation of the main switch. After the S1 switch is turned on, the resonant current decreases linearly again. Finally, when the resonant current drops to 0A, the auxiliary switch (Sx1) is turned off, which triggers the ZCS turn-off operation of the auxiliary switch. This last step is shown in Fig. 4e and 4f (corresponding to t_4 to t_6 in Fig. 3).

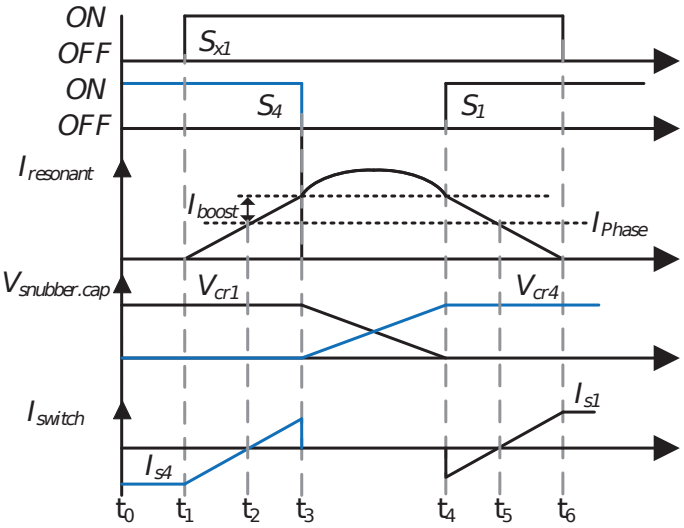

Fig. 3. ARCP ideal waveforms: Gate signals, resonant inductor current, main switch voltage, and main switch current.

C. Control of ARCP

The magnitude of the resonant current is essential for controlling the ARCP inverter. The operation of both the auxiliary and main switches is determined by the magnitude of

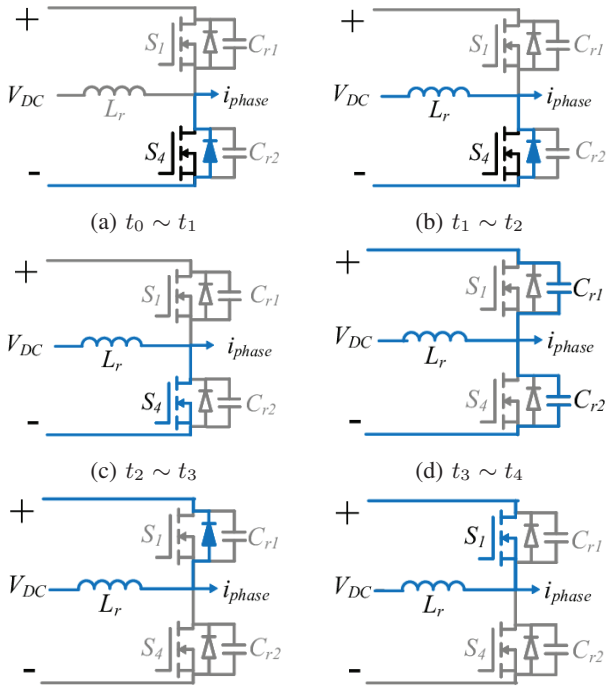

(a) $t_0 \sim t_1$ (b) $t_1 \sim t_2$

(c) $t_2 \sim t_3$ (d) $t_3 \sim t_4$

(e) $t_4 \sim t_5$ (f) $t_5 \sim t_6$

Fig. 4: ARCP commutation process: Case 1, $V_{ref} \geq V_{tri}$, $i_{phase} \geq 0$.

this current. There are two approaches to controlling the ARCP inverter: Resonant current measurement and resonant current prediction. However, the former approach is not practical due to issues with current sensor noise and delay. Therefore, the resonant current is predicted by analyzing the circuit operation. Based on this control strategy, the ARCP can be operated using either fixed-timing or variable-timing control [16]. The main difference between the two approaches is the use of the load current. Fixed-timing control does not use the load current, while variable-timing control does that into account. Fig. 5 illustrates the output waveform of the ARCP using both control methods. Fixed-timing control produces the same maximum resonant current regardless of the output load current, while the resonant current of variable-timing control depends on the output load current. Although variable-timing control is more complex than fixed-timing control, it reduces the amount of the resonant current, leading to the higher power efficiency of the ARCP inverter. Therefore, variable-timing control has been used in this paper.

D. Resonant Circuit Analysis

To determine the operation of the main and auxiliary switches, an analysis of the ARCP circuit is necessary. First, the boost current need to be evaluated such the loss contribution . The amount of the boost current is to overcome the circuit loss. This can be done using Eq. (1) [15].

$$L\frac{I_{boost}^2}{2} \geq \int i_{resonant}^2 R_{resonant.circuit} dt \tag{1}$$

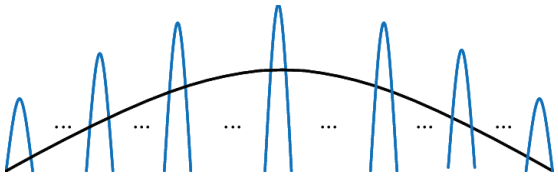

(a) Variable-timing control

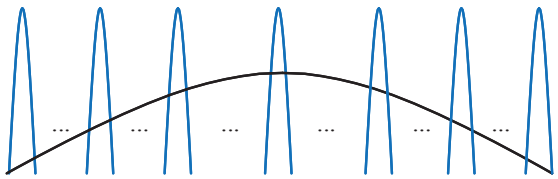

(b) Fixed-timing control

Fig. 5: Comparison ARCP control output waveform, black : phase current , blue : resonant current.

Once the boost current is determined, the time between $t_1 \sim t_3$ can be calculated using Eq. (2). The operation of the circuit during this time is shown in Fig. 4b and 4c. The resonant current during this time is affected by the resonant inductor, and the time can be expressed by Eq. (2):

$$\Delta t_{1\sim3} = 2L\frac{I_{boost} + I_{phase}}{V_{DC}} \tag{2}$$

To determine when the top switch needs to turn on, the resonant time must be calculated. This can be done through resonant circuit analysis using the equivalent circuit of the ARCP shown in Fig. 6 [14]. The response impedance Z_0 and response frequency ω_0 depend on the resonant circuit elements L_r and C_r, as shown in Eq. (3) and (4).

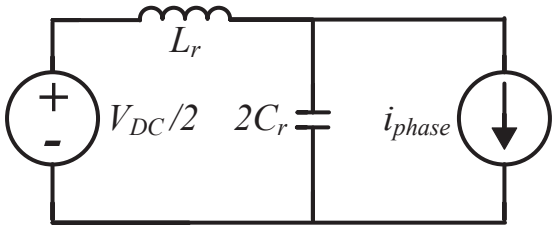

Fig. 6. Equivalent circuit of ARCP during resonance process.

$$Z_0 = \sqrt{\frac{L_r}{2C_r}} \tag{3}$$

$$\omega_0 = \frac{1}{\sqrt{2LrC_r}} \tag{4}$$

The resonant time of the ARCP inverter can be obtained using Fig. 6 and Eq. (5). Furthermore, by solving the equivalent circuit, the resonant current can be calculated using Eq. (6). From the resonant current, the maximum resonant current can be calculated.

$$t_{res} = \frac{2}{\omega_0} tan^{-1}\left(\frac{V_{dc}}{2Z_0 I_{boost}}\right) \tag{5}$$

$$i_{resonant} = I_{phase} + I_{boost}cos(\omega_0 t) + \frac{V_{dc}}{2Z_0} sin(\omega_0 t) \tag{6}$$

III. Resonant circuit element selection

The selection of resonant circuit elements is a crucial task in designing the ARCP inverter, as it determines the maximum resonant current, auxiliary circuit commutation time, and the current stress of the resonant circuit. There are several constraints to consider when selecting these elements.

The first constraint is the maximum value of the snubber capacitor. The value of the snubber capacitor is limited by system parameters such as load current, dead-time, and dc-link voltage, as shown in Eq (7).

$$C_{max} = \frac{i_{load,max} t_{time}}{V_{DC}} \tag{7}$$

The second constraint is the dead-time requirement of the system. The dead-time must exceed the resonant time of the system, which can be calculated using the equation (5) presented in the previous section. Also, the dead-time must be less than the sum of the resonant time and the boost time. The boost time can be calculated using the equation (8).

$$t_{boost} = 2L \frac{I_{boost}}{V_{DC}} \tag{8}$$

A further constraint is that the selected boost current must produce energy that exceeds the loss of the resonant circuit, and this is related to the selected resonant inductor. It can be calculated using Eq. (1).

There are three types of research that mentioned selecting resonant circuit elements in the ARCP. The first method is to use the largest snubber capacitor, which was preferred by early researchers to reduce switching losses in switches with high switching losses. However, with the development of power switch devices, smaller snubber capacitors can be used due to lower switching losses. Another method, as shown in [14], is to set the boost current to the same level as the maximum load current. However, this decision may result in an excessive boost current depending on the system. Another paper [15] has also addressed resonant circuit element selection, but it does not consider all the constraints.

This paper proposes a resonant circuit element selection process, as shown in Fig. 7. First, the system requirements for the ARCP inverter are determined, and the maximum possible snubber capacitor is calculated using Eq. (7). The temporary resonant inductor, snubber capacitor, and boost current are then determined. The resonant time and the boost time of the ARCP are calculated using the selected resonant element circuit parameters. If the dead-time does not meet the above condition, then the resonant circuit elements need to be reselected. Conversely, if the dead-time fulfills the condition, then the minimum boost current needs to be calculated. The temporary boost current is determined whether this is appropriate compared to the calculated minimum boost current. The maximum resonant current is then calculated using the selected resonant circuit elements that satisfy all constraints. This process can provide several possible resonant circuit element selections, and the optimal elements can be chosen based on the smallest resonant current.

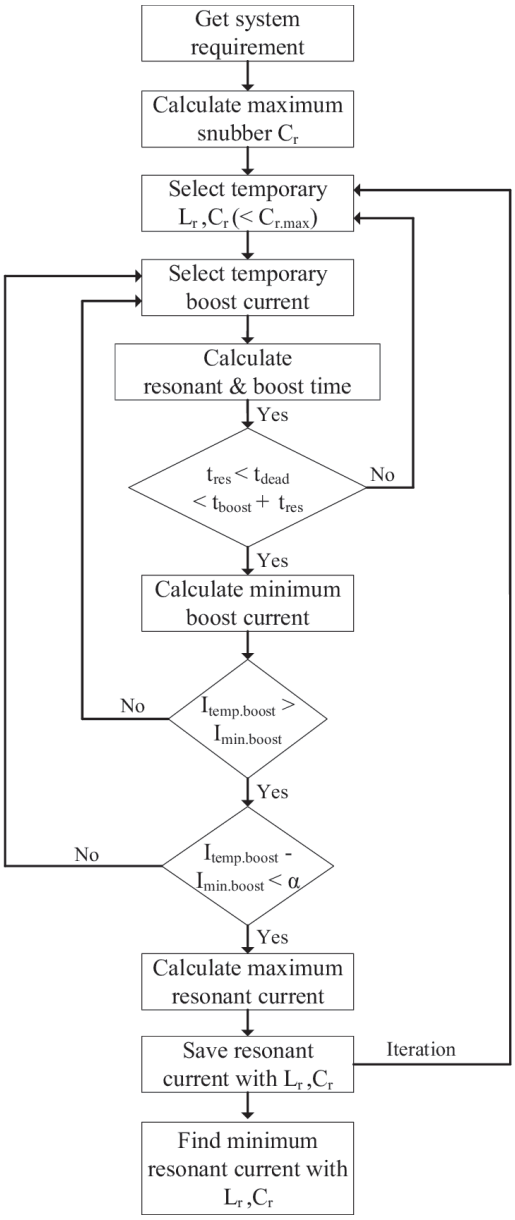

Fig. 7. Resonant circuit elements selection process.

IV. Simulation verification

A. Simulation Setup

To validate the efficacy of the suggested method for selecting resonant circuit elements, simulations were performed using different circuit configurations with the parameters listed in Table II. The main switches used were Wolfspeed SiC MOSFETs with model number C3M0016120K, and the auxiliary switches were C3M0015065K.

Three simulation cases were conducted using different methods to select the resonant circuit elements. In the first case, the maximum possible snubber capacitor value was used within the system constraints, as done in earlier research. In the second case, the method proposed in [14] was used, which sets the boost current as the maximum phase current. In the third case, the resonant circuit elements were selected using

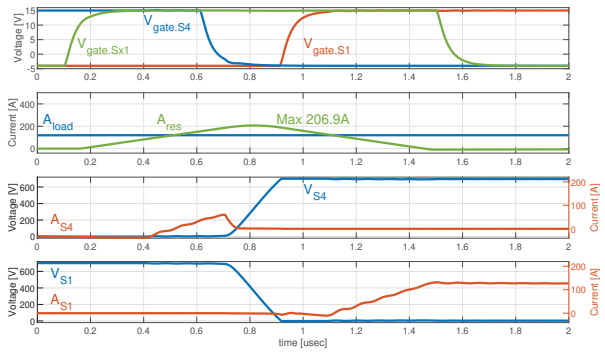

(a) Proposed method

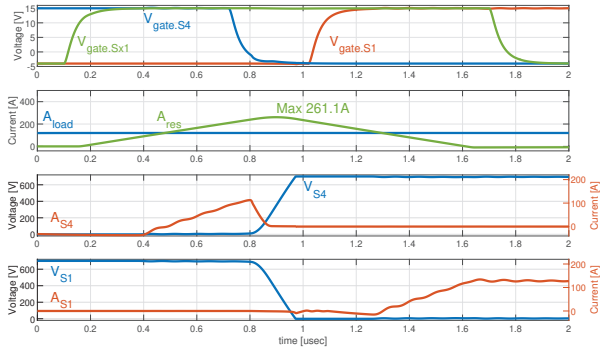

(b) Method in [14]

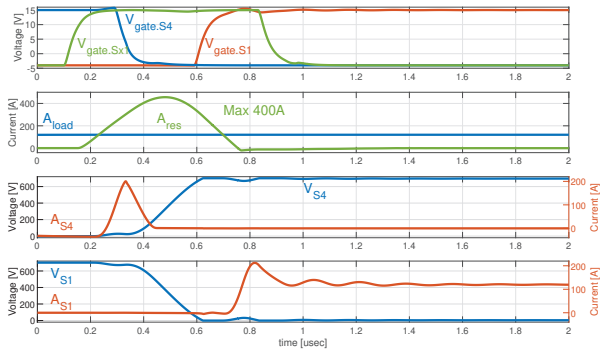

(c) Max C_r

Fig. 8: LTspice simulation results: gate signals of switches, load and resonant current, voltage and current of the main switches.

the method presented in this paper. Table III shows the selected resonant circuit elements for each method.

B. Simulation Results

Fig. 8 shows the one-cycle simulation results for the three different resonant circuit elements. The simulations were conducted in LTspice using switch models provided by Wolfspeed. Fig. 8 includes the gating signals of the main and auxiliary switches, the resonant and load current, and the voltage and current of the main switches. The simulation results show the maximum resonant current. Fig. 9 shows the comparisons of the maximum resonant current from the LTspice simulation.

TABLE II: System parameters

Parameter	Value
Max load power	45 kW
V_{dc}	700V
Fundamental frequency	60Hz
Power factor	0.8

TABLE III: Selected resonant circuit elements

Method	$L_r[uH]$	$C_r[nF]$	$I_{boost}[A]$
Proposed method	1	11.1	60
Method in [14]	0.91	13.7	120
Max C_r	0.22	52.3	170.4

The proposed method reduced the maximum resonant current by 20.8% and 48.3% compared to the [14] and Max C_r methods, respectively.

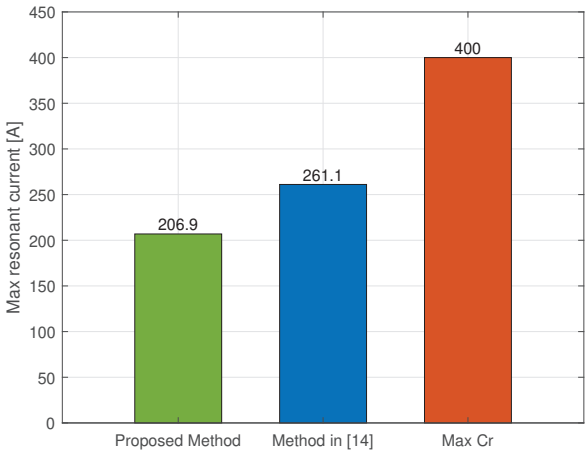

Fig. 9. Max resonant current comparison.

The proposed method improves the efficiency of three-phase inverters for two reasons. First, it reduces the loss of the resonant circuit, which affects the auxiliary switch and inductor loss. Compared to other methods, the method presented in this paper has the smallest resonant current magnitude, as shown in Fig. 8, leading to a reduction in auxiliary circuit losses and an increase in efficiency. Second, the method reduces turn-off loss of the main switch, which is related to the overlap area between the voltage and current of the switch shown in Fig. 8. The size of the snubber capacitor affects the voltage slope rate. Thus, a larger capacitor generally results in a lower voltage slope rate and reduced turn-off loss. Although the snubber capacitor size of the proposed method is smaller than that of the maximum snubber capacitor method, the proposed method achieves a smaller turn-off loss due to the smaller boost current, leading to a smaller overlap area between the switch voltage and current. The LTspice simulation results in Fig. 10 show that the proposed method reduces turn-off loss by 0.39mJ and 0.16mJ compared to the methods presented in [14] and the maximum resonant capacitor method, respec-

tively. Additionally, Fig. 11 illustrates the simulation results of the three different element selecting methods for the three-phase inverter efficiency for different load sizes with system parameters shown in Table II. The results demonstrate an improvement in efficiency ranging from 0.6% to a maximum of 9.5% compared to the previous methods.

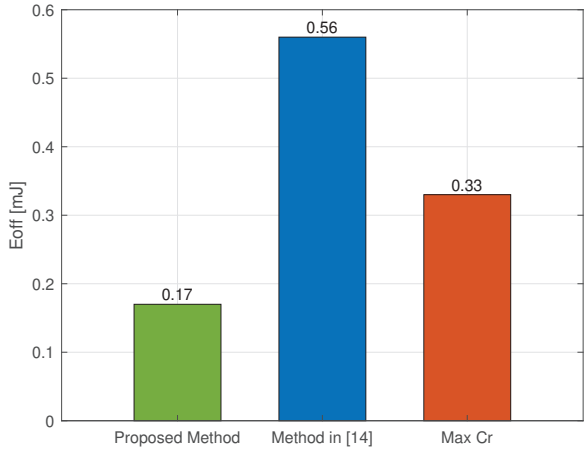

Fig. 10. Turn-off loss comparison of main switch.

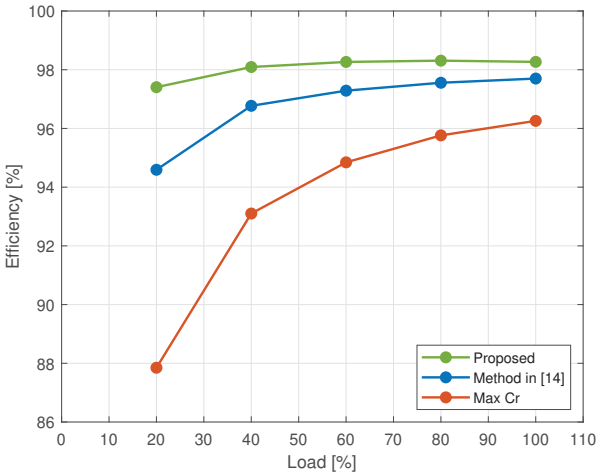

Fig. 11. Efficiency comparison.

V. Conclusion

This paper proposes an ARCP resonant circuit element selection method and compares it with the state-of-the-art methods available. LTspice and PLECS simulations of a 3-phase, 45 kW, and 700 V DC-link inverter were conducted to demonstrate that the proposed method results in the smallest resonant current, leading to reduced conduction losses in the auxiliary circuit and reduced switching losses in the main switch. Compared to other methods, the proposed method improves the overall efficiency of the ARCP inverters, making them more practical for electric vehicle applications. This proposed method is expected to contribute to the development of more efficient ARCP inverters for various applications.

References

[1] J. MoonSoo, "Industrial outlook for the second half of 2022: Automobile/mobility," HYUNDAI MOTOR SECURITIES, 2022.

[2] I. Husain, B. Ozpineci, M. S. Islam, E. Gurpinar, G.-J. Su, W. Yu, S. Chowdhury, L. Xue, D. Rahman, and R. Sahu, "Electric drive technology trends, challenges, and opportunities for future electric vehicles," *Proceedings of the IEEE*, vol. 109, no. 6, pp. 1039–1059, 2021.

[3] K. Kumar and S. B. Santra, "Performance analysis of a three-phase propulsion inverter for electric vehicles using gan semiconductor devices," *IEEE Transactions on Industry Applications*, vol. 54, no. 6, pp. 6247–6257, 2018.

[4] R. S. Krishna Moorthy, B. Aberg, M. Olimmah, L. Yang, D. Rahman, A. N. Lemmon, W. Yu, and I. Husain, "Estimation, minimization, and validation of commutation loop inductance for a 135-kw sic ev traction inverter," *IEEE Journal of Emerging and Selected Topics in Power Electronics*, vol. 8, no. 1, pp. 286–297, 2020.

[5] P. Korta, L. V. Iyer, and N. C. Kar, "Soft–switching ev traction inverter exploiting full potential of wide bandgap devices," in *IECON 2020 The 46th Annual Conference of the IEEE Industrial Electronics Society*, 2020, pp. 4703–4708.

[6] R. Li, Z. Ma, and D. Xu, "A zvs grid-connected three-phase inverter," *IEEE Transactions on Power Electronics*, vol. 27, no. 8, pp. 3595–3604, 2012.

[7] R. Li and D. Xu, "A zero-voltage switching three-phase inverter," *IEEE Transactions on Power Electronics*, vol. 29, no. 3, pp. 1200–1210, 2014.

[8] D. Xu, R. Li, N. He, J. Deng, and Y. Wu, *Basics of Soft-switching Three-phase Converters*, 2022, pp. 27–69.

[9] Q. Wang and Y. Wang, "Research on a novel high-efficiency three-phase resonant pole soft-switching inverter," *IEEE Transactions on Power Electronics*, vol. 36, no. 5, pp. 5845–5857, 2021.

[10] Z. Huang, Q. Li, and F. C. Lee, "Critical-conduction-mode-based soft-switching modulation for three-phase pv inverters with reactive power transfer capability," *IEEE Transactions on Power Electronics*, vol. 35, no. 6, pp. 5702–5713, 2020.

[11] M. Luh and T. Blank, "Auxiliary resonant commutated pole inverter (arcpi) with sic mosfets for efficient vehicle-to-grid (v2g) charging," in *2021 23rd European Conference on Power Electronics and Applications (EPE'21 ECCE Europe)*, 2021, pp. P.1–P.10.

[12] R. De Doncker and J. Lyons, "The auxiliary resonant commutated pole converter," in *Conference Record of the 1990 IEEE Industry Applications Society Annual Meeting*, 1990, pp. 1228–1235 vol.2.

[13] W. Zhou and X. Yuan, "Experimental evaluation of sic mosfets in comparison to si igbts in a soft-switching converter," *IEEE Transactions on Industry Applications*, vol. 56, no. 5, pp. 5108–5118, 2020.

[14] A. Charalambous, X. Yuan, and N. McNeill, "High-frequency emi attenuation at source with the auxiliary commutated pole inverter," *IEEE Transactions on Power Electronics*, vol. 33, no. 7, pp. 5660–5676, 2018.

[15] S. Karys, "Selection of resonant circuit elements for the arcp inverter," in *2009 10th International Conference on Electrical Power Quality and Utilisation*, 2009, pp. 1–6.

[16] K. Ma, D. Xu, T. Zhang, and S. Igarashi, "The evaluation of control strategies for auxiliary resonant commutated pole inverter," in *2009 IEEE Energy Conversion Congress and Exposition*, 2009, pp. 810–816.